Published in final edited form as:
Magn Reson Med. 2012 February ; 67(2): 389–404. doi:10.1002/mrm.23016.

On the Performance of T_2^* Correction Methods for Quantification of Hepatic Fat Content

Scott B. Reeder[1,2,3,4,*], **Emily K. Bice**[5], **Huanzhou Yu**[6], **Diego Hernando**[1], and **Angel R. Pineda**[5]

[1]Department of Radiology, University of Wisconsin, Madison, Wisconsin, USA

[2]Department of Medical Physics, University of Wisconsin, Madison, Wisconsin, USA

[3]Department of Biomedical Engineering, University of Wisconsin, Madison, Wisconsin, USA

[4]Department of Medicine, University of Wisconsin, Madison, Wisconsin, USA

[5]Department of Mathematics, California State University, Fullerton, California, USA

[6]Global MR Applied Science Laboratory, GE Healthcare, Menlo Park, California, USA

Abstract

Nonalcoholic fatty liver disease is the most prevalent chronic liver disease in Western societies. MRI can quantify liver fat, the hallmark feature of nonalcoholic fatty liver disease, so long as multiple confounding factors including T_2^* decay are addressed. Recently developed MRI methods that correct for T_2^* to improve the accuracy of fat quantification either assume a common T_2^* (single- T_2^*) for better stability and noise performance or independently estimate the T_2^* for water and fat (dual- T_2^*) for reduced bias, but with noise performance penalty. In this study, the tradeoff between bias and variance for different T_2^* correction methods is analyzed using the Cramér-Rao bound analysis for biased estimators and is validated using Monte Carlo experiments. A noise performance metric for estimation of fat fraction is proposed. Cramér-Rao bound analysis for biased estimators was used to compute the metric at different echo combinations. Optimization was performed for six echoes and typical T_2^* values. This analysis showed that all methods have better noise performance with very short first echo times and echo spacing of ∼π/2 for single- T_2^* correction, and ∼2π/3 for dual- T_2^* correction. Interestingly, when an echo spacing and first echo shift of ∼π/2 are used, methods without T_2^* correction have less than 5% bias in the estimates of fat fraction.

Keywords

noise analysis; chemical-shift imaging; T_2* correction; hepatic steatosis; Cramér-Rao bound analysis for biased estimators

[*]Correspondence to: Scott B. Reeder, MD, PhD, Department of Radiology, E3/311 CSC, University of Wisconsin, 600 Highland Avenue, Madison, WI 53792-3252, sreeder@wisc.edu.

Nonalcoholic fatty liver disease is the most common chronic liver disease in United States, affecting up to 30% of adults (1,2) and 10% of children (3–5). It is closely associated with obesity, insulin resistance, and metabolic syndrome, afflicting 60–75% of obese persons (6). Intracellular accumulation of triglycerides (hepatic steatosis) is the hallmark feature of nonalcoholic fatty liver disease. Histological analysis of steatosis based on liver biopsy is the current reference standard for assessment of hepatic fat content. However, biopsy is inherently subjective and limited, due to sampling variability, high cost, and risk of complications. For these reasons, biopsy is also poorly suited for longitudinal studies.

Recent work by multiple groups has demonstrated that MRI can accurately quantify hepatic fat content in the form of the proton density fat fraction (7–14). Accurate measurement of fat fraction requires the following confounding factors to be addressed: B_0 inhomogeneities (15,16), spectral complexity of fat (9,17), noise bias (18), T_1 bias (9,18), eddy currents (19), and T_2^* decay (9,17,20,21).

Most MRI methods that correct for T_2^* decay to improve the accuracy of fat quantification assume a common T_2^* (single- T_2^*) for water and fat (9,17,20). At relatively low (high) fat fractions, the T_2^* of water (fat) dominates, and single- T_2^* correction provide accurate measurement of fat content. However, water and fat signals have independent T_2^* in general, which may impact estimation of fat content, particularly at high fat fractions and short T_2^* (21).

To account for independent T_2^* of water and fat, O'Regan et al. (22) described a “magnitude-based” independent T_2^* correction method. Unfortunately, this approach did not account for the spectral complexity of fat, which is necessary for accurate fat quantification to avoid large errors that may be clinically significant (12,23).

Chebrolu et al. (21) recently reported a “complex-based” algorithm that uses both magnitude and phase information. They included spectral modeling in combination with independent T_2^* correction (dual- T_2^*) of water and fat. High accuracy in fat quantification with the dual- T_2^* model was demonstrated in a fat–water super-paramagnetic iron oxide phantom. However, the dual- T_2^* method (21) becomes ill-conditioned at fat fractions close to 0% or 100%, because it is not possible to estimate the T_2^* of a species accurately in the presence of noise, if that species is present in low concentrations. This instability requires constrained reconstruction methods that increase the complexity of the estimation algorithm. In addition, the dual- T_2^* model introduces additional degrees of freedom that may degrade noise performance in estimates of fat fraction.

Previous works (20,24) used the Cramér-Rao bound (CRB) analysis of unbiased estimators for characterizing the noise performance of chemical shift-based water–fat separation methods. Hernando et al. (25–27) recently compared the performance of fat quantification methods using CRB analysis of unbiased estimators. However, bias may result when no T_2^* correction or single- T_2^* correction is used. In such scenarios, the CRB analysis of biased estimators (28) may be more appropriate. One possible reason for the differences between theory and Monte Carlo simulations seen in the previous work (25–27) may have resulted from the use of CRB analysis of unbiased estimators.

Therefore, the major purpose of this work is to compare the bias and the noise performance of single- T_2^* and dual- T_2^* correction methods using CRB analysis of biased estimators for better understanding of the tradeoffs needed to improve the accuracy of fat quantification, i.e., is the reduction in bias using a dual- T_2^* model outweighed by its reduced noise performance, increased complexity and instability?

In previous noise analyses of chemical shift-based water–fat separation methods, noise performance was characterized for water-only and/or fat-only images (15,20,24). However, fat fraction is the most commonly used metric for quantifying fat content because it is independent of B_1 coil sensitivity (10–12,22,29,30). Therefore, a secondary purpose of this work was to construct a noise performance metric (NPM) for fat fraction. This metric and CRB analysis for biased estimators (CRBBE) were used to investigate the noise performance of the T_2^* correction methods. The bias and noise performance of methods without T_2^* correction were also computed for comparison.

The performance of the T_2^* correction methods analyzed for a wide range of echo combinations and the echo shifts that achieve better performance for fat fraction estimation are reported. To our knowledge, this is the first study that presents CRBBE for chemical shift-based water–fat separation methods.

Theory

Signal Equations

The signal, $s(t)$, from a volume element containing water and fat with independent T_2^* decay can be written as:

$$s(t)=\left(\rho_{\mathrm{W}} e^{i\phi_{\mathrm{W}}} e^{-R_{2,w}^{*} t}+\rho_{\mathrm{F}} e^{i\phi_{\mathrm{F}}} \sum_{p=1}^{P} r_p e^{i2\pi\Delta f_p t} e^{-R_{2f_p}^{*} t}\right) e^{i2\pi\psi t} \quad [1]$$

where ρ_W and φ_W are the magnitude and phase of water signal, ρ_F and φ_F are the magnitude and phase of fat signal. As expected from the Bloch equations and from experiments by Yu et al. (17), fat peaks have a common initial phase (φ_F) at $t = 0$. ψ is the shift (Hz) caused by local B_0 field inhomogeneities. Δf_p is the chemical shift of the p^{th} fat peak relative to water and r_p is the relative proportion of the p^{th} fat peak, such that $\sum_{p=1}^{P} r_p=1$. At clinical field strengths, the triglyceride spectrum shows at least six ($P = 6$) distinct spectral peaks (31). In this work the values of Δf_p and r_p are assumed to be known a priori, according to those reported by Hamilton et al. (31).

All the protons on a single triglyceride molecule will experience very similar magnetic field inhomogeneities (21). This is true for both microscopic and macroscopic magnetic field inhomogeneities, both of which accelerate T_2^* signal decay through enhanced dephasing of spins within an isochromat. The effects of J-coupling, which affects the apparent T_2^* decay in sequences that use refocusing pulses (e.g., fast spin-echo, point resolved spectrocopy (PRESS)), should be minimal, because our acquisition uses a low flip angle spoiled gradient echo acquisition (see below), which are unaffected by J-coupling (32,33). For all of these reasons, it should be reasonable to assume the same T_2^* for all the fat peaks, i.e., $R_{2,\mathrm{f}}^{*}=R_{2,\mathrm{fp}}^{*}$

$$s(t)=\left(\rho_{\mathrm{W}}e^{i\phi_{\mathrm{W}}}e^{-R_{2,W}^{*}t}+\rho_{\mathrm{F}}e^{i\phi_{\mathrm{F}}}e^{-R_{2,f}^{*}t}\sum_{p=1}^{P}r_{p}e^{i2\pi\Delta f_{p}t}\right)e^{i2\pi\psi t} \quad [2]$$

Equation 2 will be used as the dual- T_2^* signal model. Recently reported experiments in a fat–water–iron phantom demonstrate that the signal model in Eq. 2 accurately models the underlying physics of the water and fat signals in this phantom (21). Further, a recent report in 55 patients comparing single T_2^* correction to no T_2^* correction demonstrated excellent agreement between MRI and MR spectroscopy (MRS) (34). These data indicate that single T_2^* correction accurately modeled the physics of water and fat signal from the liver and adds indirect evidence that the T_2^* of all fat peaks are similar to each other. It is important to note, however, that in this particular group of patients, there were none who had both iron overload and severe hepatic steatosis. Dual- T_2^* modeling may still be necessary in patients with both high iron and high fat concentrations.

For N echoes measured at specific echo times t_n (n = 1,2, …, N) in the presence of Gaussian noise (35), Eq. 2 can be written in matrix form,

$$\mathbf{S}=\mathbf{A_d}\boldsymbol{\Gamma}+\varepsilon \quad [3]$$

where

$$\mathbf{A_d}=\begin{bmatrix} e^{-R_{2,W}^{*}t_1}\cos(\phi_{\mathrm{W}}+2\pi\psi t_1) & e^{-R_{2,f}^{*}t_1}\sum_{p=1}^{P}r_p\cos(\phi_F+2\pi\psi t_1+2\pi\Delta f_p t_1) \\ e^{-R_{2,W}^{*}t_1}\sin(\phi_W+2\pi\psi t_1) & e^{-R_{2,f}^{*}t_1}\sum_{p=1}^{P}r_p\sin(\phi_{\mathrm{F}}+2\pi\psi t_1+2\pi\Delta f_p t_1) \\ \vdots & \vdots \\ \vdots & \vdots \\ e^{-R_{2,W}^{*}t_N}\cos(\phi_{\mathrm{W}}+2\pi\psi t_N) & e^{-R_{2,f}^{*}t_N}\sum_{p=1}^{P}r_p\cos(\phi_{\mathrm{F}}+2\pi\psi t_N+2\pi\Delta f_p t_N) \\ e^{-R_{2,W}^{*}t_N}\sin(\phi_{\mathrm{W}}+2\pi\psi t_N) & e^{-R_{2,f}^{*}t_N}\sum_{p=1}^{P}r_p\sin(\phi_{\mathrm{F}}+2\pi\psi t_N+2\pi\Delta f_p t_N) \end{bmatrix} \quad [4]$$

and $\mathbf{S} = [s^r(t_1)\ s^i(t_1)\ \ldots\ s^r(t_N)\ s^i(t_N)]^T$, $\varepsilon=[\varepsilon_1^r\varepsilon_1^i\cdots\varepsilon_N^r\varepsilon_N^i]^T$, and $\gamma = [\rho_{\mathrm{W}}\ \rho_{\mathrm{F}}]^{\mathrm{T}} \cdot s^r(t_n)\ s^i(t_n)$ and $\varepsilon_n^r, \varepsilon_n^i$ are the real and imaginary parts of the signal and noise at the nth echo, respectively.

One challenge in the estimation of water and fat using Eq. 3 is that it becomes ill-conditioned when a voxel contains predominately water or fat (21). To avoid this instability, it can be assumed that the T_2^* of water and fat are equal (i.e., $R_{2,\mathrm{f}}^*=R_{2,\mathrm{fp}}^*=R_{2,\mathrm{w}}^*$), leading to the single- T_2^* signal model first described by Yu et al. (17) and Bydder at al. (9), i.e.,

$$s(t)=\left(\rho_{\mathrm{W}}e^{i\phi_{\mathrm{W}}}+\rho_{\mathrm{F}}e^{i\phi_{\mathrm{F}}}\sum_{p=1}^{P}r_p e^{i2\pi\Delta f_p t}\right)e^{-R_2^* t}e^{i2\pi\psi t} \quad [5]$$

For the purposes of calculating bias, we will assume the dual- T_2^* signal model in Eq. 2 to be "truth." The bias and noise performance of single versus dual- T_2^* correction will then be investigated. The bias and noise performance of methods without T_2^* correction will also be computed for comparison.

Expectation and Variance of Fat Fraction

The performance of the T_2^* correction methods is analyzed by comparing the bias and the variance in estimates of fat fraction. Fat fraction is defined as the ratio of the density of mobile fat protons (ρ_F) divided by the cumulative density of mobile water and fat protons ($\rho_W + \rho_F$). In general, there are no simple exact formulas for the expectation and variance of a quotient ($\eta=\frac{\rho_{\mathrm{F}}}{\rho_{\mathrm{W}}+\rho_{\mathrm{F}}}$) of two random variables (ρ_F, $\rho_W + \rho_F$). However, Mood et al. (36) derived approximate formulae for expectation and variance of the quotient of two random variables that have nonzero covariance. Using these formulae, the expectation value (E_η) and variance (σ_η^2) of the fat fraction becomes

$$E_\eta \approx \frac{E_{\rho_{\mathrm{F}}}}{\left(E_{\rho_{\mathrm{W}}}+E_{\rho_{\mathrm{F}}}\right)}-\frac{C+\sigma_{\rho_{\mathrm{F}}}^2}{\left(E_{\rho_{\mathrm{W}}}+E_{\rho_{\mathrm{F}}}\right)^2}+\frac{E_{\rho_{\mathrm{F}}}(\sigma_{\rho_{\mathrm{W}}}^2+\sigma_{\rho_{\mathrm{F}}}^2+2C)}{\left(E_{\rho_{\mathrm{W}}}+E_{\rho_{\mathrm{F}}}\right)^3} \quad [6]$$

$$\sigma_\eta^2 \approx \frac{\sigma_{\rho_{\mathrm{F}}}^2}{(E_{\rho_{\mathrm{W}}}+E_{\rho_{\mathrm{F}}})^2}+\frac{E_{\rho_{\mathrm{F}}}^2(\sigma_{\rho_{\mathrm{W}}}^2+\sigma_{\rho_F}^2+2C)}{(E_{\rho_{\mathrm{W}}}+E_{\rho_F})^4}-\frac{2E_{\rho_{\mathrm{F}}}(\sigma_{\rho_{\mathrm{F}}}^2+C)}{(E_{\rho_{\mathrm{W}}}+E_{\rho_{\mathrm{F}}})^3} \quad [7]$$

where the expectation of ρ_W and ρ_F are $E_{\rho W}$ and $E_{\rho F}$, the variance of ρ_W and ρ_F are $\sigma_{\rho \mathrm{W}}^2$ and $\sigma_{\rho \mathrm{F}}^2$ and the covariance between ρ_W and ρ_F is C.

For simplicity of notation, let $\mu=\frac{E_{\rho_{\mathrm{F}}}}{E_{\rho_{\mathrm{W}}}+E_{\rho_{\mathrm{F}}}}$. Note that μ does not equal E_η in general, except when there is no bias and the variance and covariance of ρ_W and ρ_F is small, as can be seen from Eq. 6. Using the expression for μ, Eq. 7 can be further simplified such that the expression for the variance of fat fraction becomes

$$\sigma_\eta^2 \approx \frac{1}{(E_{\rho_\mathrm{W}}+E_{\rho_\mathrm{F}})^2}\left[\mu^2\sigma_{\rho_\mathrm{W}}^2+(1-\mu)^2\sigma_{\rho_\mathrm{F}}^2-2C\mu(1-\mu)\right] \quad [8]$$

Equation 8 provides the expression for the variance of fat fraction given the expectation, variance and covariance of both water and fat.

Metric for Analyzing the Noise Performance of Estimation of Fat Fraction—The noise performance of fat–water decomposition has been previously analyzed using the effective number of signal averages, or NSA (15,24,37) as a metric. NSA of water (fat) is the ratio of the variance of the signal ($s(t_n)$) divided by the variance of the estimate water (fat) signal. Analogous to the NSA, we define a NPM for fat fraction as,

$$\mathrm{NPM}_\eta=\frac{1}{(E_{\rho_\mathrm{W}}+E_{\rho_\mathrm{F}})^2}\frac{\sigma^2}{\sigma_\eta^2} \quad [9]$$

This metric for noise performance of the fat fraction provides normalization of the variance of the source signal (σ_2). The NPM is the square of the ratio of the normalized measures of dispersion of probability distributions for the source signal ($\sigma/(E_{\rho\mathrm{W}} + E_{\rho\mathrm{F}})$) and fat fraction ($\sigma/1$). The normalization of dispersion of probability distribution was performed with the maximum possible values for the source signal ($E_{\rho\mathrm{W}} + E_{\rho\mathrm{F}}$) and fat fraction (1.0). If the *NSA* of water and fat magnitude signals are $\mathrm{NSA}_{\rho\mathrm{W}}$ and $\mathrm{NSA}_{\rho F}$ then using Eq. 8, the NPM_η becomes

$$\frac{1}{\mathrm{NPM}_\eta}\approx\left[\frac{\mu^2}{\mathrm{NSA}_{\rho_\mathrm{W}}}+\frac{(1-\mu)^2}{NSA_{\rho_\mathrm{F}}}-\frac{2C\mu(1-\mu)}{\sigma^2}\right] \quad [10]$$

The NPM_η provides a useful way to combine the NSA of water and fat, the covariance C between water and fat, and the variance of the signal. When C is negligible or when μ. is close to 0 or 1, the term $C\mu(1 - \mu)$ in Eq. 10 can be neglected and NPM_η become independent of SNR (σ_2). Interestingly, if $\mu = 0$ then $\mathrm{NPM}_\eta = \mathrm{NSA}_{\rho\mathrm{F}}$, i.e., when there is only water signal, the noise performance of fat fraction depends only on the NSA of fat. The opposite is true when $\mu = 100\%$. Intuitively, when the fat fraction approaches 0, the numerator in the expression for fat fraction (ρ_F) has low SNR, while the denominator ($\rho_\mathrm{W} + \rho_\mathrm{F}$) has much higher SNR and can be viewed as approximately constant. Thus, $\eta \approx \rho_\mathrm{F}/(E_{\rho\mathrm{W}} + E_{\rho\mathrm{F}})$ is nearly a scaled version of ρ_F and has similar noise performance as ρ_F. Analogously, when the fat fraction approaches 1, $\eta \approx 1 - \rho_\mathrm{W}/(E_{\rho\mathrm{W}} + E_{\rho\mathrm{F}})$ is nearly a scaled version of ρ_F is nearly a scaled and shifted version of ρ_W.

Expressions for the expectation, variance, and covariance of ρ_W and ρ_F are needed for theoretical characterization of the variance in fat fraction. The theoretical expressions for minimum possible variance in the estimates of ρ_W and ρ_F are typically calculated using CRB analysis for unbiased estimators. Pineda et al. and Reeder et al. (15,24) theoretically derived and experimentally validated the variance in the estimates of ρ_W and ρ_F for three-point chemical shift-based water–fat separation methods that correct for B_0 field inhomogeneities.

Yu et al,. (20) analyzed the noise performance of six-point fat–water estimation method that uses single- T_2^* correction.

Cramér-Rao Bound Analysis for Biased Estimators

Methods that assume a single- T_2^* model (Eq. 5) will, in general, have bias in the estimates of ρ_W and ρ_F. Similarly, parameter estimates of methods without T_2^* correction will, in general, be biased. Previous works (20,24,27) theoretically characterized the noise performance of ρ_W and ρ_F by assuming the parameters to be unbiased. However, CRBBE should be used in situations where estimators may be biased. Please see Appendix A for details of the CRBBE for fat quantification when using T_2^* correction methods.

Bias in the Estimates of ρ_W and ρ_F for Methods with No or Single- T_2^* Correction

Methods with no or single- T_2^* correction use a signal model different from that the "true" signal model, and hence in general $E(\hat{\mathbf{x}}) \neq \mathbf{x}$, for these methods. CRB of un biased estimators assume $E(\hat{\mathbf{x}})$ to be equal to $\mathbf{x}$ for all parameters. We relax this assumption and compute the bias in the estimates of ρ_W and ρ_F The estimates of the parameters φ_W, φ_F, and ψ are assumed to be unbiased and an approximate expression for the bias in R_2^* is derived below. Accurate theoretical expressions for the bias in the estimates of the nonlinear parameters φ_W, φ_F, and ψ and R_2^* is beyond the scope of this study, and, as we validate through Monte Carlo simulations, is not necessary. Please see Appendix B for details on bias calculations when using no or single T_2^* correction methods.

Materials and Methods

Estimation of Fat Fraction and R_2^* In Vivo

The tradeoff between bias and variance in the estimation of fat fraction was analyzed using three representative sets of T_2^* values to encompass a wide range of values that may be encountered physiologically.

The first set of values T_2^* were based on those measured by Schwenzer et al. (38) in 129 subjects where the average $T_2^*=28\mathrm{ms}$, and we assume that T_2^* of water and fat are equal.

T_2^* values for water and fat for the second and third cases were measured using the dual- T_2^* method (21) in two patients with severe steatosis. The second patient also has suspected hepatic iron overload from transfusional hemosiderosis. These in vivo exams were performed with institutional review board approval and informed consent and were acquired in a HIPAA compliant manner. Both the patients were scanned at 1.5 T (Signa HDx TwinSpeed, GE Healthcare, Waukesha, WI) with an eight-channel cardiac coil (GE Healthcare). Imaging parameters for the first patient included: 256 × 160, 35 × 35 cm field-of-view, 10 mm slice, 5° flip angle, ±125 kHz bandwidth, six echoes/repetition time, 13.7 ms repetition time, 1.2 ms first echo and 2.0 ms echo spacing. Imaging parameters for the second patient included: 160 × 128, 34 × 27 cm field-of-view, 8 mm slice, 12° flip angle, ±111 kHz bandwidth, six echoes/repetition time, 13.9 ms repetition time, 0.9 ms first echo, and 1.5 ms echo spacing. Two-dimensional parallel imaging with effective acceleration of

2.5 and 2.1 for the two acquisitions, respectively, was performed with autocalibrating reconstruction for Cartesian sampling (39). Both acquisitions acquired 32 slices within a 21 s breath-hold. Fat fraction and T_2^* estimates of the two methods were computed in a representative central slice from set of slices, by manually segmenting the liver tissue over the entire slice, while carefully avoiding large vessels, bile ducts and other nonhepatic tissue. The average and standard deviation were computed from the resulting histogram of T_2^* values measured from the segmented liver tissue. The identical region was used to measure T_2^* values for the single and dual T_2^* reconstructions for each patient.

Validation of Theory Using Monte Carlo Simulations

Theoretical expressions for bias and noise performance of fat fraction and the assumptions made in these calculations were validated using Monte Carlo simulations. While performing Monte Carlo validation, all the parameters were estimated independently without any assumptions regarding the bias of ρ_W, ρ_F, φ_W, φ_F, $R_{2,\mathrm{w}}^*$, $R_{2,\mathrm{f}}^*$, and ψ.

The complex MRI signal data were simulated using Eq. 2 as the true signal for fat fractions range from 0% to 100% fat. The three representative sets of T_2^* values were used. Water and fat signal magnitudes were chosen such that the value of ($\rho_W + \rho_F$) was always 100, and Gaussian noise with unit standard deviation was added to real and imaginary parts of the complex data, such that the SNR of the total water and fat signal was 100. Using the simulated noisy complex signals, estimates of ρ_W, ρ_F, φ_W, φ_F, and ψ were calculated without T_2^* correction (15). In addition, estimates of ρ_W, ρ_F, φ_W, φ_F, R_2^* and ψ were calculated using single- T_2^* correction (17,20), and finally estimates of ρ_W, ρ_F, φ_W, φ_F, $R_{2,w}^*$, $R_{2,f}^*$, and ψ were calculated using dual- T_2^* correction (21). In the Monte Carlo simulations, no field map smoothing (40) was used. Parameter estimation was repeated for 5000 independent Gaussian noise realizations for every fat fraction, and the variance of the fat fraction estimated by the three methods was computed to compare with theoretical predictions derived from CRBBE.

Echo Combination Optimization for Estimation of Fat Fraction

The CRB analysis can be performed to optimize the noise performance at different echo times in the acquisition. As the noise performance depends on fat fraction, it is important to choose a relevant range of fat fractions for this optimization. Previous studies in 110 subjects have demonstrated a range of fat fractions from 0–30% (12). Although fat fractions greater than 30% do occur, as shown by the two extreme examples in this study, they are uncommon. A vast majority of cases that we encountered at our institution have fat fractions below 30% (34). Based on these data, we performed echo time optimization for fat fraction range of 0–30%.

The impact of echo timing on bias and noise performance was computed in the following manner: the minimum NPM_η and maximum bias over the 0—30% fat fraction range was determined for a large set of echo combinations (echo time, TE_{min} = 0–2 π, ΔTE = 0–2π, and step size for both TE_{min} and ΔTE was 0.03π). From these calculations, echo combinations that maximize noise performance and minimize bias have been selected as the optimal echo combinations.

Results

Figure 1 shows the estimates of fat fraction calculated using the single and dual- T_2^* methods in the two patients, both with severe steatosis. Figure 2 shows the R_2^* values in the same patients estimated by the two methods. For the first patient, the hepatic fat fraction (%) estimated by the single and dual- T_2^* methods were 49.5 ± 4.8 and 46.5 ± 5.8, respectively. For the second patient, the hepatic fat fraction (%) was 35.6 ± 7.3 (single- T_2^* method) and 32.8 ± 7.2 (dual- T_2^* method).

The T_2^* estimated by the single- T_2^* method in the first patient was 32.3 ± 8.0ms and the corresponding T_2^* of water and fat estimated by the dual- T_2^* method were 26.4 ± 25.3 and 62.4 ± 104.4 ms, respectively. The T_2^* values estimated by the single- T_2^* method in the second patient were 11.9 ± 15.7ms and the corresponding T_2^* of water and fat estimated by the dual- T_2^* method were 12.4 ± 28.2 and 18.9 ± 27.4 ms, respectively. Note that the mean T_2^* estimates were determined from the mean of the inverse of R_2^* and not the inverse of the mean of R_2^*, which will be different in general.

The standard deviations in the estimated values of T_2^* in these patients using single and dual- T_2^* correction methods likely reflects a combination of the normal variability of T_2^* across the liver, variations related to shortening of T_2^* from external susceptibility, and from noise in the estimated R_2^* maps. Noise in the estimated R_2^* maps will depend on the T_2^* correction method used (single vs. dual), which may explain the increased variability using the dual- T_2^* correction method. Finally, it should be noted that as the region of interest used to measure the average T_2^* values is very large, the standard error on these average values is very small.

Based on the work of Schwenzer et al. (38), and measurements in these two patients, we chose T_2^* values for the three representative scenarios used in subsequent CRBBE calculations as:

1. $T_{2,w}^*=T_{2,f}^*=28\text{ms}$
2. $T_{2,w}^*=28\text{ms}, T_{2,f}^*=65\text{ms}$
3. $T_{2,w}^*=10\text{ms}, T_{2,f}^*=20\text{ms}$

Figures 3–5 plot the bias and NPM_η for methods with no, single and dual- T_2^* correction for two representative set of echo times and the three sets of T_2^* values. Six echoes with typical echo times were used with the first echo time of 1.2 ms and an echo spacing of 1.6 ms and also spacing of 2 ms. The computations were assuming chemical shift and appropriate echo times for generating a phase shift of ∼2π/ 3 and ∼π between the water peak and the main methylene peak of fat at 1.3 ppm. It is important to note that the use of phase shifts (e.g., 2π/3, π, etc.) to describe echo shifts is only valid when the two species each have a single resonance frequency, which is not the case with fat, which has at least six distinct spectral peaks. However, the use of phase shifts to describe echo times is commonly used in the literature and provides a useful intuitive basis to understand the underlying signal behavior.

Monte Carlo simulations were also performed to validate the theoretical predictions by CRBBE in Figs. 3–5. Excellent agreement between theory and Monte Carlo simulations was observed, demonstrating that assumptions made in the calculation of bias and noise performance with the CRBBE are valid. As expected, bias and noise performance are highly dependent on fat fraction, T_2^* values, and the choice of echo combinations.

From Figs. 3–5, it can be observed for all the three methods, that the minimum NPM_η (maximum variance) occurs at fat fractions close to 0%. Interestingly, when no T_2^* correction is used, the fat fraction where the minimum and maximum bias occur is highly dependent on the choice of echo combination.

Figures 6–8 show the theoretical minimum NPM_η and maximum bias for the three methods at different echo combinations. Computations were performed for fat fractions between 0% and 30% and for the three sets of T_2^* values. Interestingly, an echo spacing of ∼π/2 provides the best noise performance with single- T_2^* correction. An echo spacing of ∼2π/3 provides the best noise performance for the methods with no or dual- T_2^* correction. The echo spacings of ∼π and ∼4π/3 are the next best choices for optimal noise performance for methods without or with dual- T_2^* correction. All the three methods demonstrate tremendous improvement in noise performance with very short first echo times. Also note the difference between the noise performance at optimal echo combinations and the noise performance at a typical echo combination (shown with *) used in subjects (34).

The troughs in the two-dimensional plots for maximum bias (Figs. 6–8) identify optimal echo times for reducing bias when no T_2^* correction is used. Without T_2^* correction the echo combination with first echo time and echo spacing of (∼π/2, ∼π/2) provides less than 5% worst-case bias. The other optimal choices of first echo time and echo spacing that provide relatively smaller maximum bias (<7.5%) for methods without T_2^* correction are (∼0.75π, ∼0.80π), (∼ π, ∼0.88π), and (∼0.88π, ∼1.11π). These echo combinations are optimal for reducing bias in the estimates for fat fractions between 0% and 30%. The performance of the three T_2^* correction methods at the optimal echo combinations is compared for the complete range of fat fractions in Figs. 9 and 10.

Figure 9 plots the bias and NPM_η with the first echo time of 1.2 ms and an echo spacing of 1.1 ms. These echo times were used to generate echo combinations optimal for reducing bias for methods without T_2^* correction (Figs. 6–8). The three sets of T_2^* values were used. Results show that when a first echo time and echo spacing of (∼ π/2, ∼ π/2) are used, the estimates of fat fraction without T_2^* correction are approximately equal to the fat fractions estimated by single- T_2^* correction. Importantly, methods without T_2^* correction have less than 5% bias while providing much better noise performance than single and dual- T_2^* correction methods. Although the echo spacing of ∼π/2 is difficult to achieve for single-shot methods (all echoes in one repetition time), it is possible to achieve this spacing if interleaved echo trains are used.

Figure 10 compares the bias for methods with no, single-, and dual- T_2^* correction when using the echo combinations with first echo time and echo spacing corresponding to (∼0.75π, ∼0.80π), (∼ π, ∼∼0.88π), and (∼0.88π, ∼1.11π). The worst-case bias in the estimates of fat fraction without T_2^* correction for these echo combinations is less than 5% for fat fraction between 0% and 20% and less than 7.5% for fat fractions between 0% and 30%. Interestingly, methods without T_2^* correction have smaller bias in the estimates of fat fraction than the single- T_2^* correction methods for fat fractions between 10% and 20%.

Discussion

In this study, the tradeoff between bias and variance in the estimation of fat fraction was analyzed for different T_2^* correction methods, using CRBBE. Theoretical noise performance was compared with Monte Carlo simulations, demonstrating excellent agreement, validating the analytical expressions for CRB of biased estimators. In addition, we formulated NPM_η for the fat fraction, rather than that for water or fat signals.

We have developed an efficient framework to analyze and optimize the tradeoffs for bias and noise performance of different T_2^* correction methods. Calculations were performed using six echoes, three sets of T_2^* values encountered clinically, and over a relevant range of fat fractions. We found that using the shortest possible first TE lead to large improvements in noise performance. An echo shift of ∼π/2 provides significantly better noise performance for single- T_2^* correction, particularly when T_2^* values are short. For methods with no or dual- T_2^* correction echo shifts of ∼2π/3 provide the best noise performance, although there is a relatively broad range of echo spacings over which noise performance is similar.

In general, adding additional degrees of freedom to provide more accurate estimates of fat fraction through T_2^* correction leads to reduced bias, but at the cost of worse noise performance. The optimal choice of correction method will depend on the specific clinical scenario. For example, an application that acquires high SNR fat-fraction images or uses extensive signal averaging may be willing to trade SNR performance for improved accuracy through the use of dual- T_2^* correction. However, for most liver fat quantification applications, the SNR is generally low because rapid breathhold imaging, often with parallel imaging, is used, in combination with low flip angles (to minimize T1-related bias). Therefore, the large SNR penalty that occurs with dual- T_2^* correction may be outweighed by the reduction in bias. This is particularly true for detection of early steatosis, when concentrations of fat near 5–6% are needed to classify a patient as having abnormal levels of fat (23). For this reason, it is probably most important to have an accurate estimate of fat at low fat fractions. At low fat fractions, the bias from single- T_2^* correction methods is low and the use of dual- T_2^* may be more detrimental through large decreases in SNR performance to achieve small improvements in bias.

The bias for single- T_2^* correction, was generally small, being zero at low (∼0%) and high (∼100%) fat fractions with a maximum bias near 50%. Very interestingly, however, was the observation of "troughs" of very low maximum bias at discrete echo spacings (e.g., 0.5π, 0.88π, ∼1.11π) when no T_2^* correction was used. When very specific echo combinations were used, the bias without T_2^* correction was approximately the same as single- T_2^* correction. Importantly, the noise performance without T_2^* correction was markedly higher than single- T_2^* correction. A detailed analytical explanation for this observation is beyond the scope of this manuscript, but warrants further research to understand the basis of this observation.

In past work on the noise analysis of three-point chemical shift-based water–fat separation methods (24,37), it has been shown that a maximum effective NSA of three could be achieved for both water and fat signals, so long as the optimal choice of echo times was used (15,24). This was an intuitive result—this noise performance was equivalent to the same SNR performance by simply averaging the source images together, although without water–fat separation. Unfortunately, this analysis did not include the effects of spectral modeling of fat or the effects of T_2^* decay. Chebrolu et al. (41) recently demonstrated that inclusion of spectral modeling of fat has minimal impact on the noise performance of water signal but degrades the noise performance of the fat signal estimation. Further, Yu et al. showed that including the effects of T_2^* also reduces the noise performance in a manner that is dependent on the T_2^* value itself (17,20). For these reasons, the NPM used in this work may not have the same intuitive maximum achievable value as that for past NSA calculations. One exception is the case with 100% fat and no T_2^* correction. From Eq. 10, it can be seen that when the sample is 100% fat, the NPM only depends on the noise performance of water, and therefore, the effects of spectral modeling will not impact the NPM. In this situation, the NPM is approximately six (red curves in Figs. 3–5), which is an intuitive result that would be achieved with six well-spaced echoes, where the effects of T_2^* decay and spectral modeling are absent. Further, for the no T_2^* correction case and when the fat fraction is approximately 50%, from Eq. 10 it can be seen that NPM $\approx$ 2NPM$_{\rho w}$ = 2NPM$_{\rho f}$ ignoring the covariance term, explaining how NPM values greater than six can occur.

One important limitation of this work is that we analyzed the bias and variance in the estimates of fat fraction, separately. In some scenarios combining bias and variance as a total mean square error might be a better metric for analyzing the performance of an estimation method. However, in clinical practice, estimates of fat fraction are often analyzed by choosing a region of interest in the fat-fraction image. In such cases of clinical practice, when the mean and variance in a region of interest are computed, separating the bias and variance, as done in this study, is more useful.

A second limitation is that three assumptions were made in deriving theoretical expressions for the CRBBE. First, the expectation and variance of fat fraction are derived using the approximate formulae provided by Mood et al. (36). Second, φ_W, φ_F, and ψ were assumed to be accurately estimated without bias by the three T_2^* correction methods. Third, we used an approximate expression for bias in R_2^*. The later two assumptions were made to avoid recursive theoretical equations for the bias in the estimates of fat fraction. However, close agreement between Monte Carlo simulations and theoretical noise performance demonstrates that these assumptions were valid for analyzing the estimation of fat fraction over the range of parameters tested.

An additional limitation of this study is that the dual- T_2^* signal model (Eq. 2) assumes that the T_2^* of all fat peaks are equal, and that the spectral model of fat is known. The assumptions regarding uniform T_2^* of the fat peaks is probably reasonable, based on the fact that all protons on a triglyceride molecule experience the same B_0 field inhomogeneity and that J-coupling effects are negligible when using low flip angle spoiled gradient echo imaging (32,33). In addition, Hamilton et al. (31) recently characterized the relative frequencies and amplitudes of liver triglycerides in 121 patients with liver disease. In this study, they characterized the triglyceride spectrum and also demonstrated minimal variability of the spectral model of fat between patients (i.e., all subjects had very similar triglyceride spectra). Perhaps most importantly, however, recently reported data in a fat–water–iron phantom demonstrate that dual- T_2^* correction with spectral modeling of fat accurately models the underlying physics of the water and fat signals from this phantom (21). Further, recently reported data in 55 patients (none of whom had both iron overload and high fat concentration) demonstrate excellent agreement between MRS and MRI with spectral modeling and single- T_2^* correction, providing indirect evidence that the T_2^* of all triglyceride peaks are very similar (34). However, it is important to stress that the major purpose of this work was not to investigate the validity of the single and dual- T_2^* signal models but rather investigate the relative tradeoffs in noise performance between the two signal models.

Finally, the analysis was limited to six echo acquisitions, although analysis of other echo train lengths is warranted. However, additional optimization and validation is beyond the scope of this work.

In conclusion, we have presented a rigorous framework for analyzing the bias and noise performance of fat quantification using complex chemical shift-based water–fat separation methods. As part of this framework, we formulated a NPM for estimation of fat fraction as the parameter of interest and validated the use of CRB for biased estimators to determine the minimum variance of the estimates of fat fraction. Using this framework, we compared three T_2^* correction methods to examine the tradeoffs among bias, noise performance, and instability of algorithms. We found that for typical acquisition parameters over a wide range of fat fractions, significantly better tradeoff between bias and variance is achieved with the single- T_2^* correction method. In addition, we demonstrated that at very discrete echo spacings, methods without T_2^* correction achieve similar bias to that of single- T_2^* correction methods but with greatly improved noise performance. Future work will use the dual- T_2^* correction method to measure differences in T_2^* between water and fat to help determine the role and need for dual- T_2^* correction for in vivo fat quantification in larger populations. In addition, detailed analysis of the discrete echo spacings that provide small bias with no T_2^* correction will also be pursued.

Acknowledgments

The authors wish to thank GE Healthcare for their support.

Grant sponsor: NIH Clinical and Translational Science Award (to University of Wisconsin ICTR); Grant number: 1UL1RR025011; Grant sponsor: NIH; Grant numbers: RC1EB010384, R01 DK083380-01A1, and R01 DK088925-01.

Appendix A

Cramér-Rao Bound Analysis for Biased Estimators

Let x = $[\rho_W\ \rho_F\ \varphi_W\ \varphi_F\ R^*_{2,W}\ R^*_{2,f}\ \psi]^T$ be the vector representation of the parameters to be estimated. If $\hat{\mathbf{x}}$ is the estimate of **x**, then the bias **b** in $\hat{\mathbf{x}}$ is $E(\hat{\mathbf{x}}) - \mathbf{x}$ and the covariance **C** of $\hat{\mathbf{x}}$ is $E\{[\hat{\mathbf{x}} - E\hat{\mathbf{x}}][\hat{\mathbf{x}} - E(\hat{\mathbf{x}})]^T\}$. If $E(\hat{\mathbf{x}}) = \mathbf{x}$, then the estimator is unbiased. This assumption is appropriate when the signal model used by the estimation method and the truesignal model are the same. In this study, we assume the dual- T_2^* signal model to be truth. Hence, for dual-T_2^* correction we perform the CRB analysis of unbiased estimators and the minimum variance on each parameter is given by the diagonal elements of the inverse of the Fisher information matrix **F** (24,42), whose (*k, l*)th element is given by the equations:

$$\mathbf{F}_{kl}=\frac{\left[\mathbf{A}_{\mathbf{d}}^{\mathrm{T}}\mathbf{A}_{\mathbf{d}}\right]_{kl}}{\sigma^2};\text{for } k=1,2 \text{ and } l=1,2 \quad \text{[A1]}$$

$$\mathbf{F}_{kl}=\frac{\left[\mathbf{A}_{\mathbf{d}}^{\mathrm{T}}\frac{\partial \mathrm{A}_d}{\partial x_l}\boldsymbol{\Gamma}\right]_{kl}}{\sigma^2};\text{for } k=1,2 \text{ and } l=3,4,\ldots,7 \quad \text{[A2]}$$

$$\mathbf{F}_{kl}=\frac{\left[\boldsymbol{\Gamma}^{\mathrm{T}}\frac{\partial \mathbf{A}_{\mathbf{d}}^{\mathrm{T}}}{\partial x_k}\frac{\partial \mathbf{A}_{\mathbf{d}}}{\partial x_l}\boldsymbol{\Gamma}\right]_{kl}}{\sigma^2};\text{for } k=3,4,\ldots,7 \text{ and } l=3,4,\ldots,7 \quad \text{[A3]}$$

where σ^2 is the variance of the noise in a source image ($s(t)$). x_k and x_l are the *k*th and *l*th vector elements of **x**. If the parameter estimation method uses a signal model different than true signal model, then generally $E(\hat{\mathbf{x}}) \neq \mathbf{x}$. In this case, the estimator is biased. The theoretical expressions for the minimum possible variance in the biased estimates of the parameters are computed using CRBBE, i.e.,

$$C \geq \mathbf{C} \geq \left[\mathbf{I}+\frac{\partial \mathbf{b}}{\partial \mathbf{x}}\right]\mathbf{F}^{-1}\left[\mathbf{I}+\frac{\partial \mathbf{b}}{\partial \mathbf{x}}\right]^T \quad \text{[A4]}$$

where $\frac{\partial \mathbf{b}}{\partial \mathbf{x}}$ is the partial derivative of the bias with respect to the parameters (**x**). To simplify notation below, we define $D=\frac{\partial \mathbf{b}}{\partial \mathbf{x}}$. The theoretical minimum value for the variance in the biased estimates of the parameters is given by the diagonal elements of **C**, the covariance matrix. The theoretical minimum variance of the parameters estimated by the CRBBE using Eq. 12 becomes equal to the minimum variance estimated by the CRB theory of unbiased estimators, when **D** is zero, or in other words, when the estimator is unbiased.

Fat fraction is the metric of interest, therefore, $c_{11}\left(\sigma^2_{\rho W}, c_{12}\left(C\right)\right.$, and $c_{22}\left(\sigma^2_{\rho F}\right)$ are the only elements of **C** (Eq. 14) that need to be derived. The only elements of **D** that must be computed are the partial derivatives of the bias in ρ_W and ρ_F with respect to ρ_W, ρ_F, φ_W, φ_F, $R^*_{2,w}$, $R^*_{2,f}$ and ψ. All elements of **F** are required

Appendix B

Bias for Methods with No or Single- T_2^* Correction

Expressions for the minimum variance in estimates of ρ_W and ρ_F depend on their bias. To calculate the partial derivatives in Eq. 14, analytical expressions for the bias in ρ_W and ρ_F are required. Let $\hat{\Gamma_{\mathbf{n}}}$ and $\hat{\Gamma_{\mathbf{s}}}$ be the vector representation of the biased estimates of water and fat signal magnitudes by methods without T_2^* correction and with single- T_2^* correction, respectively. Then $\hat{\Gamma_{\mathbf{n}}}$ and $\hat{\Gamma_{\mathbf{s}}}$ are given by the equations

$$\hat{\mathbf{\Gamma}}_{\mathbf{n}}=\left(\mathbf{A_n}^{\mathrm{T}}\mathbf{A_n}\right)^{-1}\mathbf{A_n}^{\mathbf{T}}\mathbf{A_d}\mathbf{\Gamma} \quad \text{[B1]}$$

$$\hat{\mathbf{\Gamma}}_{\mathbf{s}}=\left(\mathbf{A_s}^{\mathbf{T}}\mathbf{A_s}\right)^{-1}\mathbf{A_s}^{\mathbf{T}}\mathbf{A_d}\mathbf{\Gamma} \quad \text{[B2]}$$

$\mathbf{A_n}$ is obtained from $\mathbf{A_d}$ in Eq. 4 by substituting $R^*_{2,w}$ and $R^*_{2,f}$ with zero. Similarly, $\mathbf{A_s}$ is obtained from $\mathbf{A_d}$ by substituting $R^*_{2,w}$ and $R^*_{2,f}$ with R^*_2. Equations 15 and 16 provide expressions for bias in ρ_W and ρ_F. These equations were used for deriving theoretical bounds for the minimum possible variance in the parameter estimates.

Approximate Expression for R_2^*

An analytical expression for the bias in the R_2^* estimated by the single- T_2^* model is needed to calculate the partial derivative on the bias in Eq. 14. The R_2^* estimated by the single- T_2^* model will have zero bias at 0 and 100% fat fractions because there is only one component (water or fat). However, bias will be nonzero between these extremes. A linear approximation that satisfies the above condition for the R_2^* is $(1-\eta)R^*_{2,w}+\eta R^*_{2,f}$. A more accurate, nonlinear approximation for R_2^* can be derived by equating Eqs. 2 and 5, and assuming that φ_W, φ_F, and ψ have already been demodulated, i.e.,

$$e^{-R_2^* t} \approx \frac{\rho_{\mathrm{W}} e^{-R^*_{2,w}t}+\rho_{\mathrm{F}}|c_f|e^{-R^*_{2,f}t}}{\rho_{\mathrm{W}}+\rho_{\mathrm{F}}|c_f|} \quad \text{[B3]}$$

where $c_f=\sum_{p=1}^{P} r_p e^{i2\pi\Delta f_p t}$ for simplicity. If we define $\hat{\rho}_{W,s}$ and $\hat{\rho}_{F,s}$ to be the biased estimates of the water and fat signal magnitudes of the single- T_2^* correction method, then using $\hat{\rho}_{W,s} + \hat{\rho}_{F,s}|C_f|$ in the denominator would provide a more accurate expression for R_2^*. Equation 17 provides an approximate analytical expression for the R_2^* decay term to conduct partial differentiation of the bias, **b**.

References

1. Chitturi S, Abeygunasekera S, Farrell GC, Holmes-Walker J, Hui JM, Fung C, Karim R, Lin R, Samarasinghe D, Liddle C, Weltman M, George J. NASH and insulin resistance: insulin hypersecretion and specific association with the insulin resistance syndrome. Hepatology. 2002; 35:373–379. [PubMed: 11826411]
2. Harrison SA, Neuschwander-Tetri BA. Nonalcoholic fatty liver disease and nonalcoholic steatohepatitis. Clin Liver Dis. 2004; 8:861–879. ix. [PubMed: 15464659]
3. Papandreou D, Rousso I, Mavromichalis I. Update on non-alcoholic fatty liver disease in children. Clin Nutr. 2007; 26:409–415. [PubMed: 17449148]
4. Tominaga K, Kurata JH, Chen YK, Fujimoto E, Miyagawa S, Abe I, Kusano Y. Prevalence of fatty liver in Japanese children and relationship to obesity. an epidemiological ultrasonographic survey. Dig Dis Sci. 1995; 40:2002–2009. [PubMed: 7555456]
5. Schwimmer JB, Deutsch R, Kahen T, Lavine JE, Stanley C, Behling C. Prevalence of fatty liver in children and adolescents. Pediatrics. 2006; 118:1388–1393. [PubMed: 17015527]
6. Angulo P, Lindor KD. Non-alcoholic fatty liver disease. J Gastroenterol Hepatol. 2002; 17(Suppl):S186–S190. [PubMed: 12000605]
7. Rydell J, Knutsson H, Pettersson J, Johansson A, Farneback G, Dahlqvist O, Lundberg P, Nystrom F, Borga M. Phase sensitive reconstruction for water/fat separation in MR imaging using inverse gradient. Med Image Comput Comput Assist Interv. 2007; 10(Pt 1):210–218. [PubMed: 18051061]
8. Cowin GJ, Jonsson JR, Bauer JD, Ash S, Ali A, Osland EJ, Purdie DM, Clouston AD, Powell EE, Galloway GJ. Magnetic resonance imaging and spectroscopy for monitoring liver steatosis. J Magn Reson Imaging. 2008; 28:937–945. [PubMed: 18821619]
9. Bydder M, Yokoo T, Hamilton G, Middleton MS, Chavez AD, Schwimmer JB, Lavine JE, Sirlin CB. Relaxation effects in the quantification of fat using gradient echo imaging. Magn Reson Imaging. 2008; 26:347–359. [PubMed: 18093781]
10. Hines CD, Yu H, Shimakawa A, McKenzie CA, Brittain JH, Reeder SB. T1 independent, T2* corrected MRI with accurate spectral modeling for quantification of fat: validation in a fat-water-SPIO phantom. J Magn Reson Imaging. 2009; 30:1215–1222. [PubMed: 19856457]
11. Guiu B, Petit JM, Loffroy R, Ben Salem D, Aho S, Masson D, Hillon P, Krause D, Cercueil JP. Quantification of liver fat content: comparison of triple-echo chemical shift gradient-echo imaging and in vivo proton MR spectroscopy. Radiology. 2009; 250:95–102. [PubMed: 19092092]
12. Yokoo T, Bydder M, Hamilton G, Middleton MS, Gamst AC, Wolfson T, Hassanein T, Patton HM, Lavine JE, Schwimmer JB, Sirlin CB. Nonalcoholic fatty liver disease: diagnostic and fat-grading accuracy of low-flip-angle multiecho gradient-recalled-echo MR imaging at 1.5 T. Radiology. 2009; 251:67–76. [PubMed: 19221054]
13. Hu HH, Kim HW, Nayak KS, Goran MI. Comparison of fat–water MRI and single-voxel MRS in the assessment of hepatic and pancreatic fat fractions in humans. Obesity (Silver Spring). 2010; 18:841–847. [PubMed: 19834463]
14. Hines CD, Yu H, Shimakawa A, McKenzie CA, Warner TF, Brittain JH, Reeder SB. Quantification of hepatic steatosis with 3-T MR imaging: validation in ob/ob mice. Radiology. 2010; 254:119–128. [PubMed: 20032146]
15. Reeder SB, Pineda AR, Wen Z, Shimakawa A, Yu H, Brittain JH, Gold GE, Beaulieu CH, Pelc NJ. Iterative decomposition of water and fat with echo asymmetry and least-squares estimation (IDEAL): application with fast spin-echo imaging. Magn Reson Med. 2005; 54:636–644. [PubMed: 16092103]
16. Hernando D, Haldar JP, Sutton BP, Ma J, Kellman P, Liang ZP. Joint estimation of water/fat images and field inhomogeneity map. Magn Reson Med. 2008; 59:571–580. [PubMed: 18306409]
17. Yu H, Shimakawa A, McKenzie CA, Brodsky E, Brittain JH, Reeder SB. Multiecho water–fat separation and simultaneous R2* estimation with multifrequency fat spectrum modeling. Magn Reson Med. 2008; 60:1122–1134. [PubMed: 18956464]
18. Liu CY, McKenzie CA, Yu H, Brittain JH, Reeder SB. Fat quantification with IDEAL gradient echo imaging: correction of bias from T(1) and noise. Magn Reson Med. 2007; 58:354–364. [PubMed: 17654578]

19. Yu, H.; Shimakawa, A.; Reeder, S.; McKenzie, C.; Brittain, J. Magnitude fitting following phase sensitive water–fat separation to remove effects of phase errors; Proceedings of the 17th Scientific Meeting of ISMRM; Honolulu, HI. 2009; p. 461
20. Yu H, McKenzie CA, Shimakawa A, Vu AT, Brau AC, Beatty PJ, Pineda AR, Brittain JH, Reeder SB. Multiecho reconstruction for simultaneous water–fat decomposition and T2* estimation. J Magn Reson Imaging. 2007; 26:1153–1161. [PubMed: 17896369]
21. Chebrolu VV, Hines CD, Yu H, Pineda AR, Shimakawa A, McKenzie CA, Samsonov A, Brittain JH, Reeder SB. Independent estimation of T*2 for water and fat for improved accuracy of fat quantification. Magn Reson Med. 2010; 63:849–857. [PubMed: 20373385]
22. O'Regan DP, Callaghan MF, Wylezinska-Arridge M, Fitzpatrick J, Naoumova RP, Hajnal JV, Schmitz SA. Liver fat content and T2*: simultaneous measurement by using breath-hold multiecho MR imaging at 3.0 T—feasibility. Radiology. 2008; 247:550–557. [PubMed: 18349314]
23. Szczepaniak LS, Nurenberg P, Leonard D, Browning JD, Reingold JS, Grundy S, Hobbs HH, Dobbins RL. Magnetic resonance spectroscopy to measure hepatic triglyceride content: prevalence of hepatic steatosis in the general population. Am J Physiol Endocrinol Metab. 2005; 288:E462–E468. [PubMed: 15339742]
24. Pineda AR, Reeder SB, Wen Z, Pelc NJ. Cramer-Rao bounds for three-point decomposition of water and fat. Magn Reson Med. 2005; 54:625–635. [PubMed: 16092102]
25. Hernando, D.; Liang, ZP.; Kellman, P. Comparison of magnitude and complex data fitting for quantitative water/fat imaging; Proceedings 18th Scientific Meeting, International Society for Magnetic Resonance in Medicine; Stockholm, Sweden. 2010; p. 5098
26. Hernando, D.; Liang, ZP.; Kellman, P. Modeling of T2* decay in water/ fat imaging: comparison of one-decay and two-decay models; Proceedings 18th Scientific Meeting, International Society for Magnetic Resonance in Medicine; Stockholm, Sweden. 2010; p. 5095
27. Hernando D, Liang ZP, Kellman P. Chemical shift–based water/fat separation: a comparison of signal models. Magn Reson Med. 2010; 64:811–822. [PubMed: 20593375]
28. Eldar YC. Minimum variance in biased estimation: bounds and asymptotically optimal estimators. IEEE Trans Signal Processing. 2004; 52:1915–1930.
29. Hussain HK, Chenevert TL, Londy FJ, Gulani V, Swanson SD, McKenna BJ, Appelman HD, Adusumilli S, Greenson JK, Conjeevaram HS. Hepatic fat fraction: MR imaging for quantitative measurement and display—early experience. Radiology. 2005; 237:1048–1055. [PubMed: 16237138]
30. Reeder, S.; Hines, C.; Yu, H.; McKenzie, C.; Brittain, J. On The definition of fat-fraction for in vivo fat quantification with magnetic resonance imaging; Proceedings of the 17th Scientific Meeting, International Society for Magnetic Resonance in Medicine; Honolulu, Hawaii. April 2009; p. 211
31. Hamilton G, Yokoo T, Bydder M, Cruite I, Schroeder ME, Sirlin CB, Middleton MS. In vivo characterization of the liver fat (1)H MR spectrum. NMR Biomed. 2010 Epub ahead of print.
32. de Graaf R, Rothman D. In vivo detection and quantification of scalar coupled (1)H NMR resonances. Concepts Magn Reson. 2001; 13:32–76.
33. Hamilton G, Middleton MS, Bydder M, Yokoo T, Schwimmer JB, Kono Y, Patton HM, Lavine JE, Sirlin CB. Effect of PRESS and STEAM sequences on magnetic resonance spectroscopic liver fat quantification. J Magn Reson Imaging. 2009; 30:145–152. [PubMed: 19557733]
34. Meisamy S, Hines CD, Hamilton G, Sirlin CB, McKenzie CA, Yu H, Brittain JH, Reeder SB. Quantification of hepatic steatosis with T1-independent, T2*-corrected MR imaging with spectral modeling of fat: blinded comparison with MR spectroscopy. Radiology. 2011; 258:767–775. [PubMed: 21248233]
35. McVeigh ER, Henkelman RM, Bronskill MJ. Noise and filtration in magnetic resonance imaging. Med Phys. 1985; 12:586–591. [PubMed: 4046992]
36. Mood, AM.; Graybill, FA.; Boes, DC. Introduction to the theory of statistics. NY: McGraw-Hill; 1974.
37. Glover GH. Multipoint Dixon technique for water and fat proton and susceptibility imaging. J Magn Reson Imaging. 1991; 1:521–530. [PubMed: 1790376]

38. Schwenzer NF, Machann J, Haap MM, Martirosian P, Schraml C, Lie-big G, Stefan N, Haring HU, Claussen CD, Fritsche A, Schick F. T2* relaxometry in liver, pancreas, and spleen in a healthy cohort of one hundred twenty-nine subjects-correlation with age, gender, and serum ferritin. Invest Radiol. 2008; 43:854–860. [PubMed: 19002057]
39. Brau AC, Beatty PJ, Skare S, Bammer R. Comparison of reconstruction accuracy and efficiency among autocalibrating data-driven parallel imaging methods. Magn Reson Med. 2008; 59:382–395. [PubMed: 18228603]
40. Yu H, Reeder SB, Shimakawa A, Brittain JH, Pelc NJ. Field map estimation with a region growing scheme for iterative 3-point water-fat decomposition. Magn Reson Med. 2005; 54:1032–1039. [PubMed: 16142718]
41. Chebrolu VV, Yu H, Pineda AR, McKenzie CA, Brittain JH, Reeder SB. Noise analysis for 3-point chemical shift-based water-fat separation with spectral modeling of fat. J Magn Reson Imaging. 2010; 32:493–500. [PubMed: 20677283]
42. Van Trees, HL. Detection, estimation, and modulation theory. New York: Wiley; 1968.

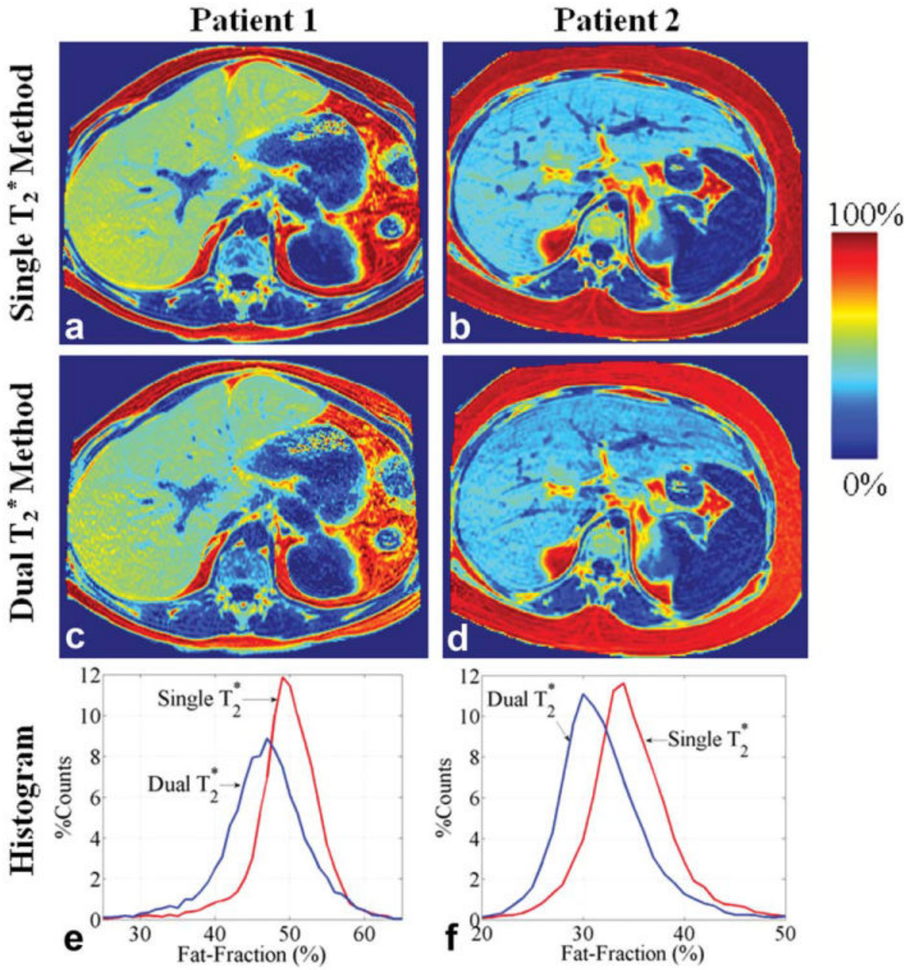

Fig. 1.

In vivo quantification of fat fraction (%) using the single (**a**, **b**) and dual (**c**, **d**) T_2^* correction methods in two patients with severe steatosis. The hepatic fat fractions were manually segmented to avoid large vessels and biliary structures. Histogram plots (bin size = 1%) of the hepatic fat fractions estimated by the two methods are shown in (**e**) and (**f**). Data for the second patient were provided by Dr. Shreyas S. Vasana-wala.

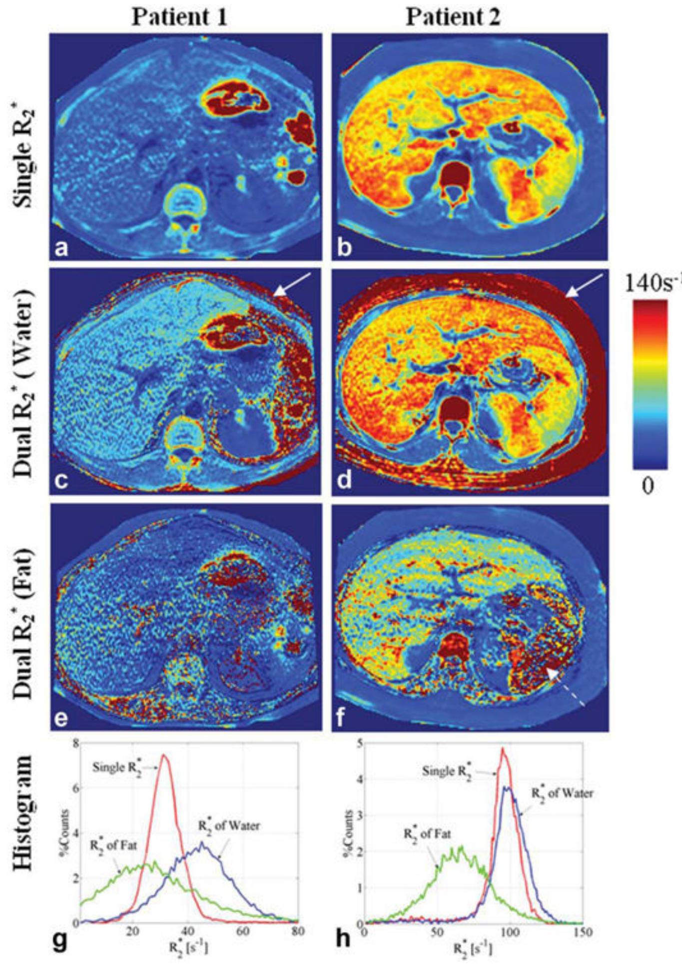

Fig. 2.

Estimates of R_2^* in the same patients, shown in Fig. 1, using the single (**a**, **b**) and dual (**c-f**) T_2^* correction methods. Histogram plots (bin size = 1 s^{-1}) of the R_2^* estimates by the two methods in the liver, manually segmented avoiding large vessels and biliary structures, are shown in (**g**, **h**). The dual T_2^* method is unstable when one species dominants the voxel as seen by the estimates of the R_2^* of water in subcutaneous fat (solid arrows) and the R_2^* of fat estimated in the spleen (dashed arrow). The higher R_2^* values in the second patient are consistent with known concomitant iron overload in addition to steatosis. Data for the second patient were provided by Dr. Shreyas S. Vasanawala.

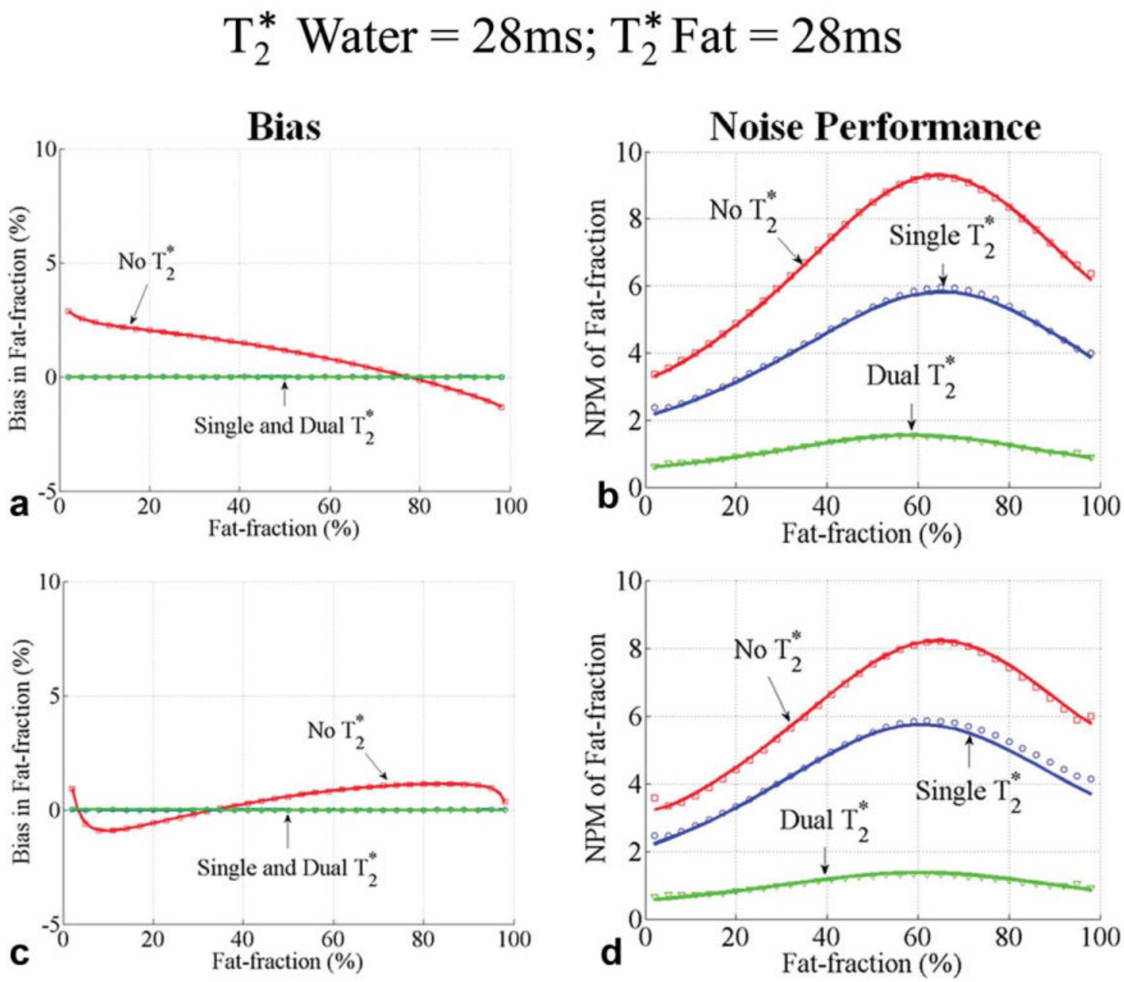

Fig. 3.

Bias (**a**, **c**) and noise performance (**b**, **d**) in estimation of fat fraction using six echoes without T_2^* correction, single and dual T_2^* correction, when the water and fat signals have the same T_2^* (28 ms). Two sets of representative echo times were used: a first echo time of 1.2 ms and an echo spacing of 2 ms were used in (a, b) and a first echo time of 1.2 ms and an echo spacing of 1.6 ms were used in (c, d). Close agreement between theoretical calculations (lines) and Monte Carlo simulations (□, ○, and ▽) is seen. The bias is zero for only dual T_2^* methods because the T_2^* is the same for water and fat (28 ms). A large decrease in SNR performance occurs due to the additional degrees of freedom for dual T_2^* correction method.

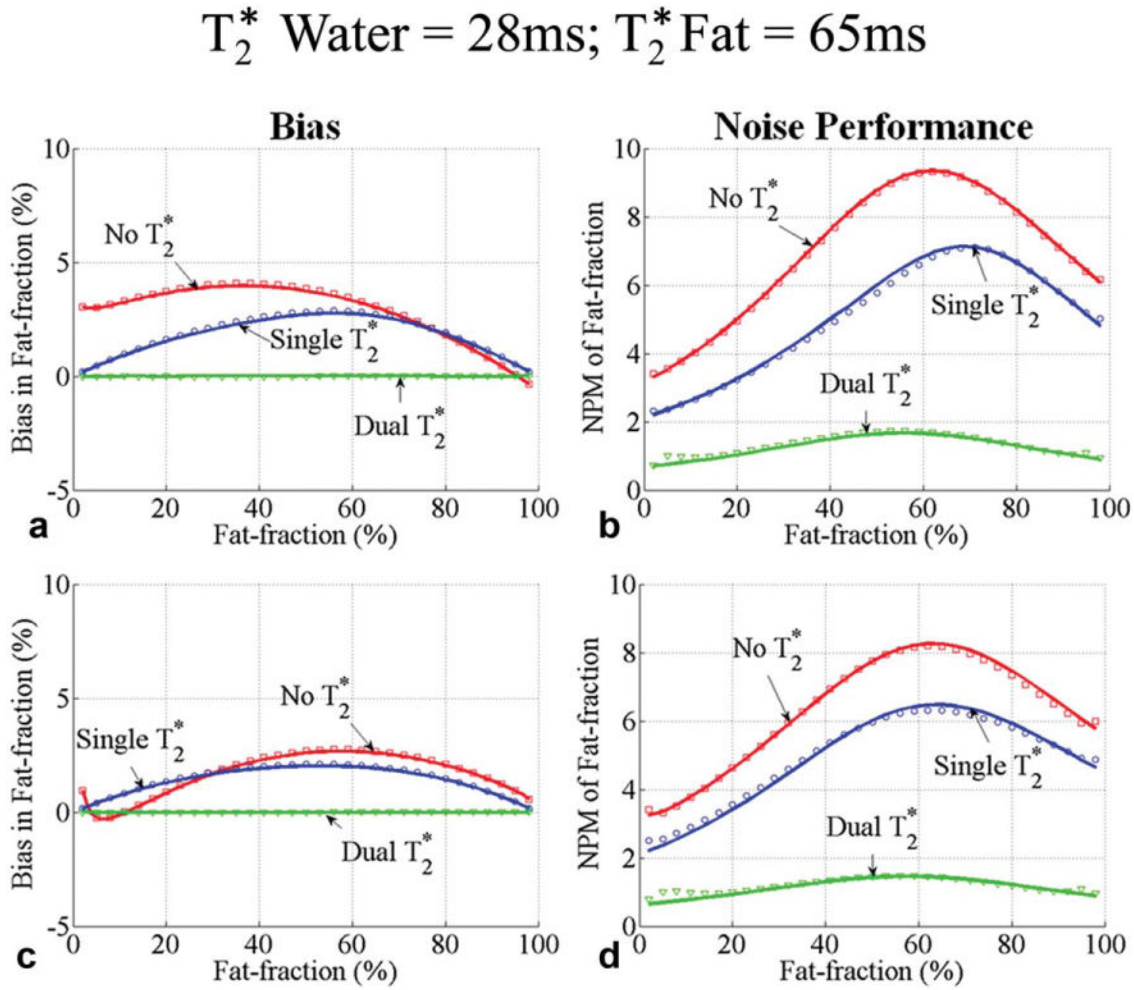

Fig. 4.

Bias (**a**, **c**) and noise performance (**b**, **d**) in fat-fraction estimation using six echoes without T_2^* correction, single, and dual T_2^* correction, when the T_2^* of water is 28 ms and T_2^* of fat is 65 ms. Two sets of representative echo times were used: a first echo time of 1.2 ms and an echo spacing of 2 ms were used in (a, b) and a first echo time of 1.2 ms and an echo spacing of 1.6 ms were used in (c, d). Close agreement between theoretical calculations (lines) and Monte Carlo simulations (□, ○ and ▽) is seen. Also note that the bias for methods without T_2^* correction depends heavily on the choice of echo timing. The bias is zero only for dual T_2^* correction. A large decrease in SNR performance occurs when adding additional degrees of freedom for the dual T_2^* correction method in an attempt to reduce bias.

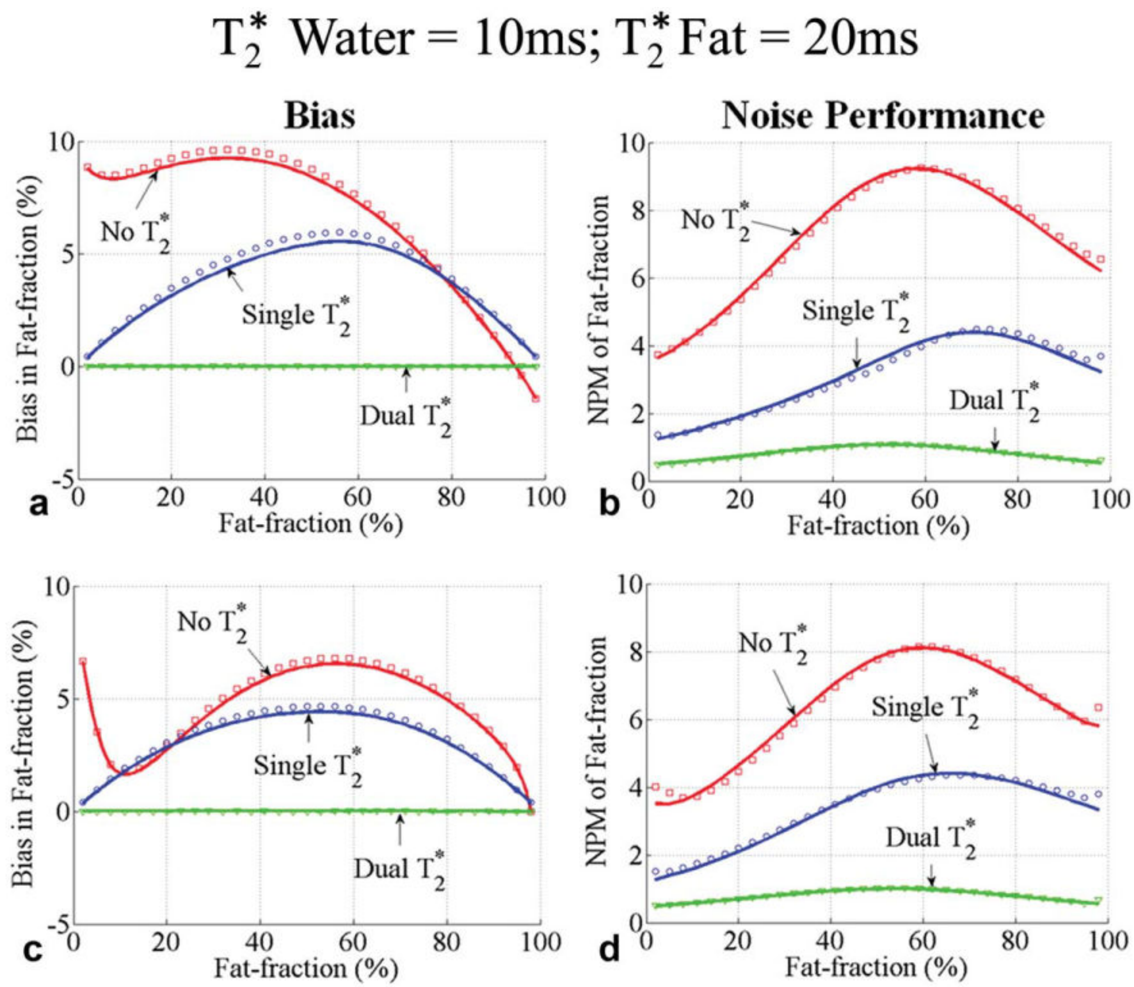

Fig. 5.

Bias (**a**, **c**) and noise performance (**b**, **d**) in fat fraction estimation using six echoes without T_2^* correction, single, and dual T_2^* correction, when the T_2^* of water is 10 ms and T_2^* of fat is 20 ms. Two sets of representative echo times were used: a first echo time of 1.2 ms and an echo spacing of 2 ms were used in (a, b) and a first echo time of 1.2 ms and an echo spacing of 1.6 ms were used in (c, d). Close agreement between theoretical calculations (lines) and Monte Carlo simulations (□, ○ and ▽) is seen. The bias is zero for only dual T_2^* correction. Note that the bias for methods without T_2^* from iron overload. A large decrease in SNR performance occurs when adding additional degrees of freedom for single and dual T_2^* correction methods in an attempt to reduce bias.

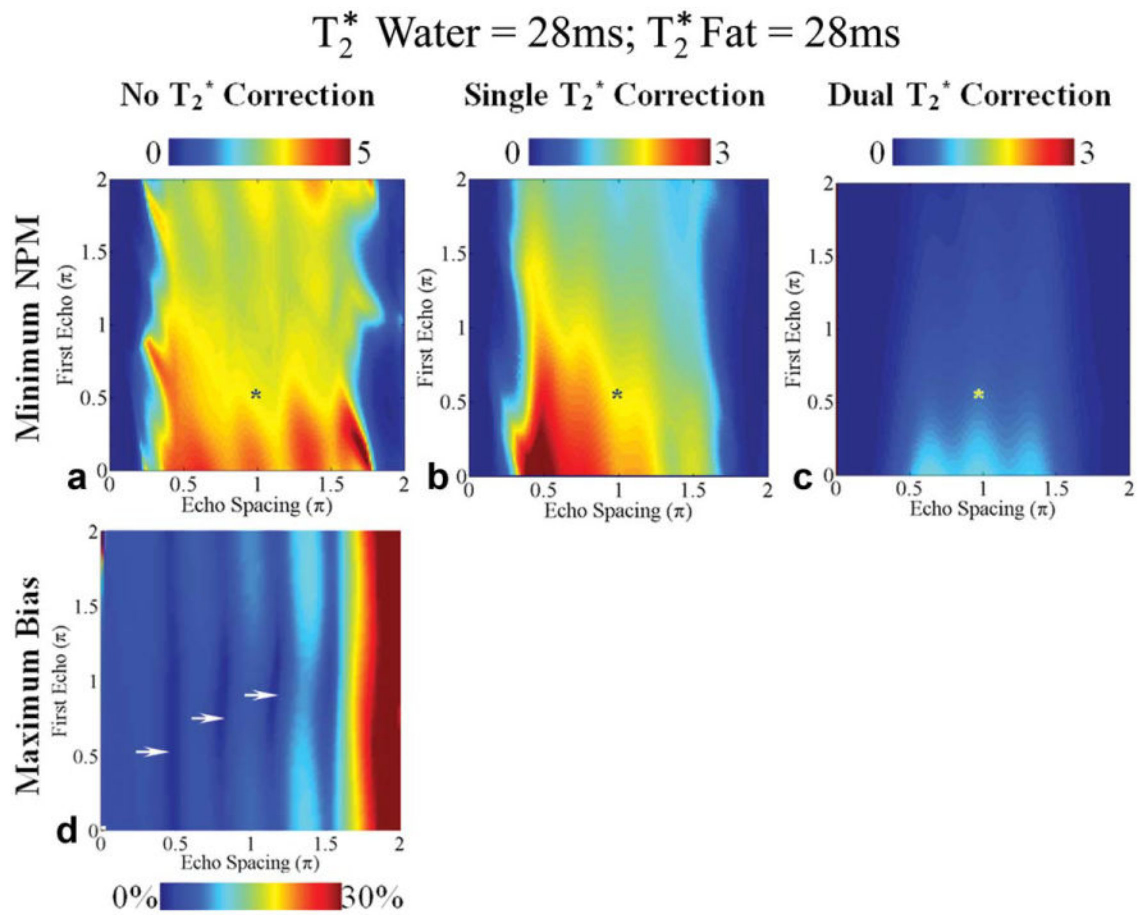

Fig. 6.

Worst-case noise performance (**a-c**) and bias (**d**) in the estimation of fat fraction using six echoes for fat fractions between 0% and 30% for methods without T_2^* correction (a, d), single T_2^* correction (b), and dual T_2^* correction (c) when the water and fat signals have the same T_2^* (28 ms). First echo time and the echo spacing are represented using the phase difference (multiples of π) between water and the main fat peak at 1.3 ppm. Note that the color bar scales for worst-case NPM for methods with T_2^* correction range from 0 to 3 and for methods without T_2^* correction range from 0 to 5. A typical echo combination used in subjects is shown with an asterisk (*). The optimal echo spacing for best noise performance for methods with no or dual T_2^* correction is ~2π/3. An echo spacing of ~π/2 provides the best noise performance for single T_2^* correction. Single and dual T_2^* correction methods have no bias in this case because the T_2^* of water and fat are equal (28 ms). The regions with small worst-case bias for methods without T_2^* correction are shown by arrows.

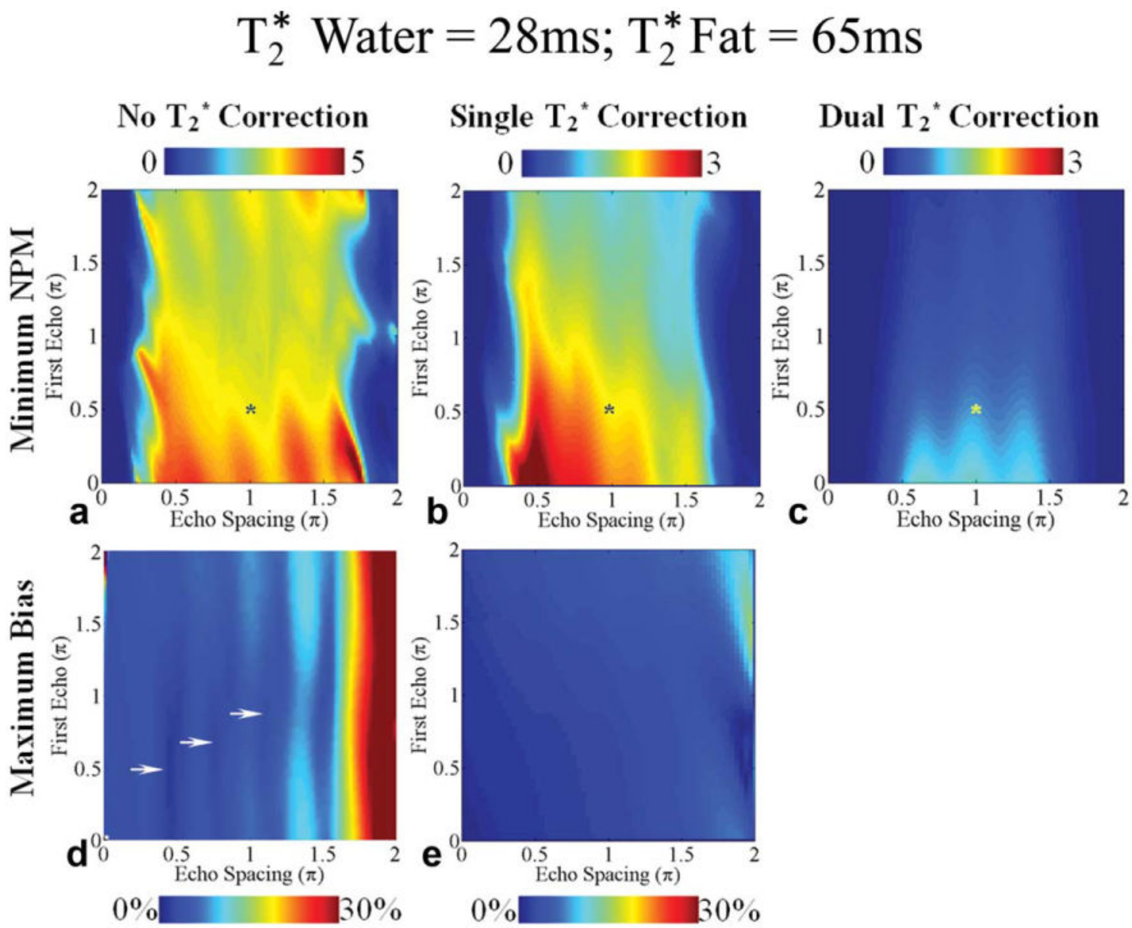

Fig. 7.

Worst-case noise performance (**a-c**) and bias (**d**, **e**) in the estimation of fat fraction using six echoes for fat fractions between 0% and 30% for methods without T_2^* correction (a, d), single, (b) and dual T_2^* correction (c) when T_2^* of water is 28 ms and T_2^* of fat is 65 ms. First echo time and the echo spacing are represented using the phase difference (multiples of π) between water and the main fat peak at 1.3 ppm. Note that the color bar scales for worst-case NPM for methods with T_2^* correction range from 0 to 3 and for methods without T_2^* correction range from 0 to 5. A typical echo combination used in subjects is shown with an asterisk (*). The optimal echo spacing for best noise performance for methods with no or dual T_2^* correction is ∼2π/3. An echo spacing of ∼ π/2 provides the best noise performance for single T_2^* correction. Only dual T_2^* correction methods have no bias in this case. The regions with small worst-case bias for methods without T_2^* correction are shown by arrows.

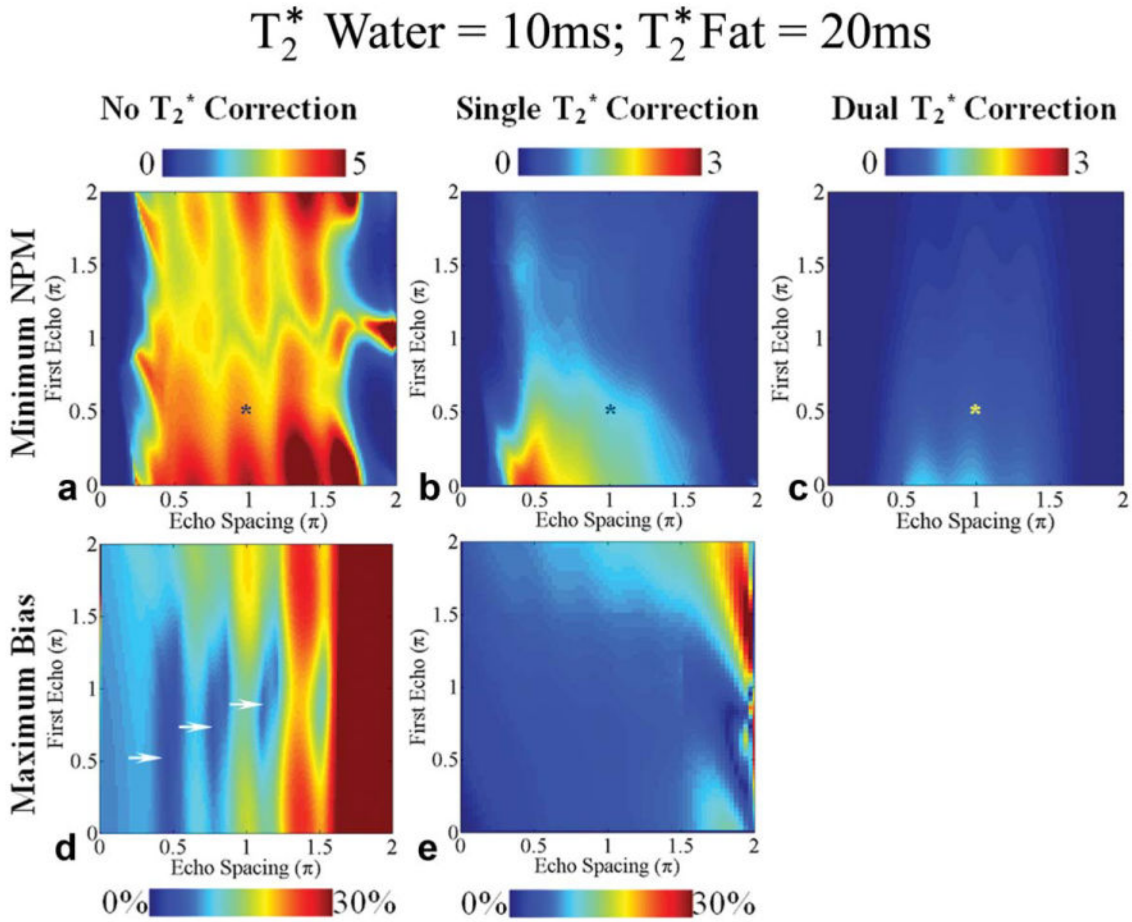

Fig. 8.

Worst-case noise performance (**a-c**) and bias (**d**, **e**) in the estimation of fat fraction using six echoes for fat fractions between 0% and 30% for methods without T_2^* correction (a, d), single, (b) and dual T_2^* correction (c) when T_2^* of water is 10 ms and T_2^* of fat is 20 ms. First echo time and the echo spacing are represented using the phase difference (multiples of π) between water and the main fat peak at 1.3 ppm. Note that the color bar scales for worst-case NPM for methods with T_2^* correction range from 0 to 3 and for methods without T_2^* correction range from 0 to 5. A typical echo combination used in subjects is shown with an asterisk (*). The optimal echo spacing for best noise performance for methods with no or dual T_2^* correction is ∼2π/3. An echo spacing of ∼π/2 provides the best noise performance for single T_2^* correction. Only dual T_2^* correction methods have no bias in this case. The regions with small worst-case bias for methods without T_2^* correction are shown by arrows. Among the regions pointed to by the arrows, the region close to the first echo time and echo spacing of ∼π/2 represents the optimum choice of echo times for reducing bias without T_2^* correction because it has lowest value for maximum bias (<4% error).

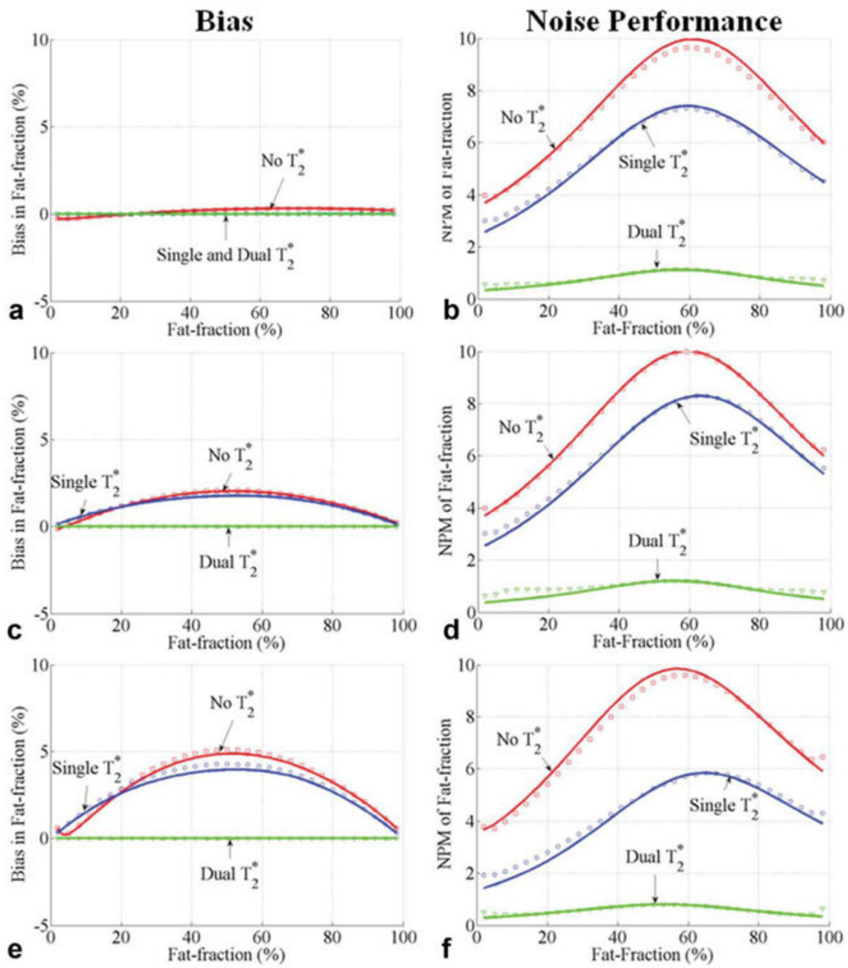

Fig. 9.

Bias (**a**, **c**, **e**) and noise performance (**b**, **d**, **f**) in estimation of fat fraction with the first echo time and echo spacing of (∼ π/2, ∼ π/2) for 0–100% fat fractions. Results from Figs. 6 to 8 show that these echo combinations have less than 4% worst-case bias for methods without T_2^* correction for fat fractions between 0% and 30%. A first echo time of 1.2 ms, an echo spacing of 1.1 ms, and six echoes were used. The performance of methods without T_2^* correction, single, and dual T_2^* correction for three sets of T_2^* are shown. The following combinations of T_2^* values were used: T_2^* of 28 ms for both water and fat (a, b), T_2^* of 28 ms for water and 65 ms for fat (c, d), and T_2^* of 10 ms for water, and 20 ms for fat (e, f). Close agreement between theoretical calculations (lines) and Monte Carlo simulations (□,○ and ▽]) is seen. Interestingly, the bias for methods with single and no T_2^* correction is approximately the same for this echo combination. In addition, methods without T_2^* correction have significantly better noise performance. This specific echo combination may provide a combination of low bias and excellent noise performance if no T_2^* correction is used.

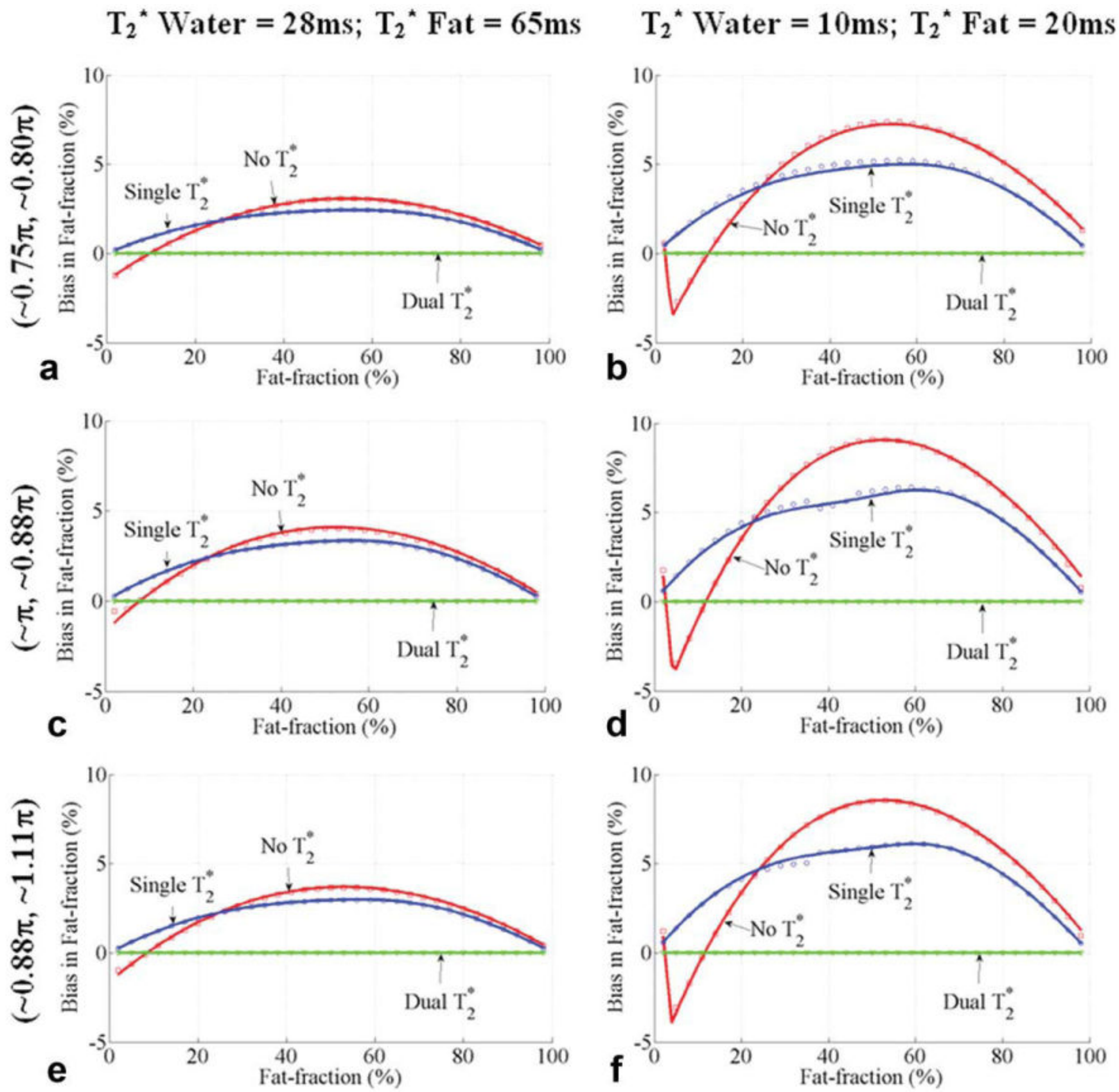

Fig. 10.

Bias in the estimates of fat fraction with the first echo time and echo spacing of (∼0.75π, ∼0.80π), (∼ π, ∼0.88π), and (∼0.88π, ∼ 1.11 π) for 0–100% fat fractions. Results from Figs. 6 to 8 show that these echo combinations have small worst-case bias without T_2^* correction for fat fractions between 0% and 30%. These echo combinations use echo spacing longer than π/2. Six echoes were used, as well as three representatives sets of T_2^* for water and fat: T_2^* of 28 ms for water and fat (the bias without T_2^* correction was less than 2% for all the three optimum echo combinations and is not shown); T_2^* of 28 ms for water and 65 ms for fat (**a**, **c**, **e**); T_2^* of 10 ms for water and 20 ms for fat (**b**, **d**, **f**). Close agreement between theoretical calculations (lines) and Monte Carlo simulations (□, ○ and ▽) is seen. Note that methods without T_2^* correction provide less than 5% worst-case bias for fat fractions between 0% and 20% and have smaller bias than methods with single T_2^* correction for fat fractions between 10% and 20%.